Large-scale investigation of wave dampening characteristics of organic, artificial floating islands

Landmann, Jannis ; Hammer, Tim C.; Günther, Henning ; Hildebrandt, Arndt

DOI
10.1016/j.ecoleng.2022.106691

Publication date
2022

Document Version
Final published version

Published in
Ecological Engineering

Citation (APA)
Landmann, J., Hammer, T. C., Günther, H., & Hildebrandt, A. (2022). Large-scale investigation of wave dampening characteristics of organic, artificial floating islands. *Ecological Engineering*, *181*, Article 106691. https://doi.org/10.1016/j.ecoleng.2022.106691

Ecological Engineering 181 (2022) 106691

Contents lists available at ScienceDirect

Ecological Engineering

journal homepage: www.elsevier.com/locate/ecoleng

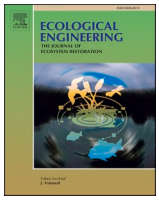

Large-scale investigation of wave dampening characteristics of organic, artificial floating islands

Jannis Landmann [a,*], Tim C. Hammer [b], Henning Günther [c], Arndt Hildebrandt [a]

[a] Leibniz Universität Hannover, Ludwig-Franzius-Institute for Hydraulic, Estuarine and Coastal Engineering, Nienburger Straße 4, 30167 Hannover, Germany
[b] Delft University of Technology, Department of Hydraulic Engineering, Stevinweg 12628 CN Delft, the Netherlands
[c] Hochschule für Technik und Wirtschaft Dresden, Fakultät Landbau/Umwelt/Chemie, Fachgebiet Garten- und Landschaftsbau, Friedrich-List-Platz 1, 01069 Dresden, Germany

ARTICLE INFO

Keywords:
Artificial floating islands
Wave dampening
Reflection coefficient
Transmission coefficient
Large scale experiment

ABSTRACT

The concept of floating vegetation-based islands for the bioremediation of aquatic ecosystems is well known. Less so, their hydrodynamic capabilities regarding the damping performance, positional stability and water-structure interactions. To this end, physical model tests with fully organic, reed-based gabions were carried out in a large-scale facility in this study. The initial, reflected, and transmitted waves were recorded and analyzed regarding transmission and reflection coefficients. A motion tracking system was utilized to allow for an investigation regarding the motion of the artificial floating islands under waves. The results show that the artificial floating islands significantly dampen shorter waves with a wave period of $T \leq 2.25$ s. The transmission of the incident waves is reduced by 50% for the smallest wave periods ($T = 1.5$ s). The incident waves are reflected between 20 and 50% for the same wave period. The incident wave energy is dissipated by up to 85% for the smallest wave height and period (H = 0.10 m, $T = 1.5$ s). The comparable performance regarding more traditional floating breakwaters is discussed as well as the width of the structure as the key parameter for the layout of artificial floating islands in rivers and still waters regarding the damping performance.

1. Introduction

Ship-induced waves are a major anthropogenic load scenario acting on fauna and flora along dam-regulated rivers and canals. In contrast to wind-induced waves, ship waves have different characteristic properties to which natural vegetation is not adapted (Silinski et al., 2015). The longer periods and larger wave heights of these wave systems in comparison to wind-induced waves, adversely affect flora and fauna along the shoreline, which can lead to a loss of ecological habitats and natural revetments. It is critical to recognize and mitigate these effects of ship-induced waves to protect inland water biodiversity in the future (Gabel et al., 2017). Therefore, different protection approaches are needed to counter these negative impacts. Artificial floating islands (AFIs) are a promising method to dampen ship waves and protect the shoreline apart from traditional revetments. AFIs are fully organic structures, with no added buoyancy and remain afloat due to a self-replenishing gas reservoir created by anaerobic decomposition and aerenchyma tissue of the used reeds (Hogg and Wein, 1988). The aerenchyma tissue is less dense than water and provides buoyancy (Kaul, 1974). The stems of the plants remain mainly above the water level, while their roots grow downwards through the reed body into the water column. This hydroponic growth pattern enables the plants to take their nutrition directly from the water column in the absence of a subsoil (Hubbard, 2010; Kadlec and Wallace, 2009). Studies regarding the ecosystem services provided by AFIs showed that pollutants can be removed via the suspended root system of the AFIs due to nutrient and metal uptake as metals dissolved in the water body are recovered by the AFIs, leading to a reduction of pollutants and therefore to an ecological improvement of the whole ecosystem (Barco and Borin, 2020; Headley and Tanner, 2012; Kadlec and Bevis, 2009; Ma et al., 2021; Machado Xavier et al., 2018; Zhu et al., 2011). Furthermore, AFIs support the development of a biofilm compromised of fungi, bacteria and algae, which have been shown to remove nitrogen from a water body (Chang et al., 2012). Regarding wildlife habitat purposes, AFIs have been shown to offer breeding space, away from land-born predators, for birds on the reed structure itself (Shealer et al., 2006) as well as shading, removal options for fish-farming effluents and cover for aquatic species (Nakamura and Mueller, 2008; Saviolo Osti et al., 2020). The societal effects

* Corresponding author.
E-mail address: landmann@lufi.uni-hannover.de (J. Landmann).

https://doi.org/10.1016/j.ecoleng.2022.106691
Received 6 September 2021; Received in revised form 4 May 2022; Accepted 17 May 2022
Available online 27 May 2022

regarding the public perception of coastal habitat loss and habitat creation using AFIs has also been studied (Ware and Callaway, 2019). This closer look at the available literature reveals that the wave damping through AFIs is not investigated in depth or substantially covered in the scientific literature for the needed combination of ecological and hydrodynamic details. This is also mentioned in a current review by Vymazal et al. (2021), who state the research in regard to design and operational parameters is still lacking.

Focusing on these hydrodynamics aspects, an analogy can be drawn to floating breakwaters, which are known to attenuate waves through a number of dissipative mechanisms, e.g. reflection, wave breaking, friction, vortex formation and shedding, jet mixing and resonance (Sawaragi, 1995). The AFIs tested in this study are in their shape similar to box-type breakwaters, which mainly attenuate waves by reflection (Dai et al., 2018; McCartney, 1985). Examples for this breakwater have been investigated thoroughly. Theoretical research regarding the performance and occurring mooring forces has been conducted by Adee (1974, 1975, 1976). Williams et al. (2000) used 2D-potential theory to study the performance of two floating double-box breakwaters. Their results indicated that the geometry and spacing between two floating breakwaters as well as the mooring are important for the performance of the breakwater. Numerical research has also been conducted by Rahman et al. (2006), who modelled the nonlinear, dynamic responses and mooring forces of submerged breakwaters using the volume of fluid method. They investigated wave breaking and vortices as waves were passing by the wave breaker using the Navier-Stokes equation. They validated their model with small scale tests in a wave tank. In a study by Diamantoulaki and Angelides (2010), the overall performance of an array of floating breakwaters connected by hinges was evaluated numerically. They concluded that an increase in the number of hinges may improve the overall effectiveness of the breakwater in dependence on the ratio of breakwater width and wavelength. These flexible modes where also included in a physical 1:20 model by Loukogeorgaki et al. (2014) who investigated structural response and effectiveness of a moored floating breakwater. They found that the structural response was strongly dependent on the incident wave period while wave height and obliquity mainly effect the response in low frequency ranges. Further examples comparable to the AFIs, include floating tire breakwaters (Bishop, 1985; Giles and Sorensen, 1978), which attenuate waves mainly by friction along its wetted surface and also by disturbing the wave particle orbits, or perforated horizontal floating plate breakwaters (Arunachalam and Raman, 1982), where wave attenuation is strongly influenced by wave steepness and relative length of the breakwater. Mani (1991) tested a trapezoidal floating wave breaker with and without pipes lowered into the water. The results show that with the inclusion of the pipes, comparable to submerged canopies or roots, the width requirement for effective wave attenuation can be significantly reduced. In a study by Dong et al. (2008) box-type breakwaters in three configurations, i.e. as a single box, a double box and a board net, were experimentally tested in a wave-current flume. Their results suggested deep-water capabilities of the latter configuration. Wang and Sun (2010) presented a novel floating breakwater consisting of diamond shaped blocks. They showed that it can reduce the incident wave height by dissipating more wave energy than reflecting it. Xiang et al. (2019) used a MIKE21 SW model to determine the optimal location of artificial islands in a plain reservoir to dissipate waves, where AFIs could be used.

Such dissipative mechanisms can be projected to the AFIs as their effectiveness also depends on parameters such as the shape, widths, draught, mass, the mooring system, the water depth at the installation site and the incident waves. However, it remains unclear to date, how appropriate the use of AFIs are as breakwaters. This is the most important gap of knowledge for the further development of AFIs as revetment or breakwater options.

Based on this shortcoming, a comprehensive experimental program has been devised to further the understanding of the complex flow problematic regarding the interaction of AFIs and waves. Thus, the general objective of this study is to quantify the hydrodynamic impact of the AFIs in a large-scale facility and to elucidate the processes regarding wave-structure interaction and overall performance. The specific objectives of these tests are to:

- conduct systematic and reproducible tests to analyze the alterations of hydrodynamic interaction of regular waves with AFIs in a large-scale facility.
- separate and quantify the wave-dampening properties of the AFIs, thereby considering the reflection, transmission, and overall movement of the AFIs.
- determine and discuss the governing wave and structure parameters regarding wave dampening and structure movement as well as the main dissipation mechanisms of the AFIs.

Quantification of hydrodynamic performance and the accompanying discussions of gained insights allow for an ecological and low-cost way to plan and install vegetated floating islands along waterways to serve as additional revetments. Researchers, industry and public officials can use this to form a fact-based decision on the effectiveness of AFIs apart from their known ecological advantages.

2. Materials and methods

Full-scale experiments were carried out in the Large Wave Flume (GWK) of the Coastal Research Center in Hannover. The GWK is 307 m long, 5 m wide and 7 m deep. The hydraulically driven machine shaft (900 kW) has a maximum stroke of ±2.10 m for regular waves and can generate maximum wave heights of up to 2.0 m. The water level was set to a constant 4.90 m during testing. The test field is positioned between flume meters 101.0–120.0. The slope of the dissipative beach at the far end of the flume was set to a steepness of 1:11. Fig. 1 shows a depiction of the flume with the location of the test field and the AFIs in a side view.

2.1. Test setup

The AFIs developed by Günther (2013) are comprised of individual reed gabions, which consist mainly of common reed (*Phragmites australis*), native to the African and Eurasian continents. The reed gabions have a dimension of 100 cm × 100 cm and a maximal height of 25 cm with a wire mesh used for stabilization of the reed blades. Before conducting the research in the wave flume, we measured culm density (188 pcs ± 95), height of above-ground culms (87 cm ± 9) with a cover ratio of 38%, and root length (18 cm ± 5). This indicates a young, growing stock. Further information regarding *P. australis* and its structure, growth dynamics, biomass, root system, and ability to remove pollutants is available (Eller et al., 2017; Engloner, 2009; Marzec et al., 2018; Soukup et al., 2002). The average dry density of *Phragmites* is ~0.16 g/cm^3. The weight of a single reed gabion body is 39.95 kg. The initial draught in dry condition is 3.93 cm. The average density increases up to 1.06 g/cm^3 for wet conditions with 80% water-saturation and the weight increase up to 196.8 kg. In wet conditions, the draught is near equal to the height of the reed gabion. The gabions were planted and placed in a water basin two vegetation periods before the start of the experiments themselves to ensure fully grown and biologically settled conditions. The gabions maintain buoyancy due to aerenchyma tissue in the *Phragmites*, which has a lower density than water, and trapped swamp gas, mainly composed of CH^4, $C0^2$ and N^2 (Günther, 2013). The gas is formed during anaerobic decomposition of organic matter and is captured by the intertwined root system and the body of the reed gabion.

During testing, the swamp gas underneath each gabion was simulated by panels of extruded polystyrene (XPS) hard foam. The XPS-panels with dimensions of 100 cm × 40 cm × 2 cm and a density of 0.050 g/cm^3 were chosen due to their robust, water-repellent characteristics and the comparable buoyancy of the trapped swamp gas. The panel was fixed with threaded rods, which were pushed through the AFI

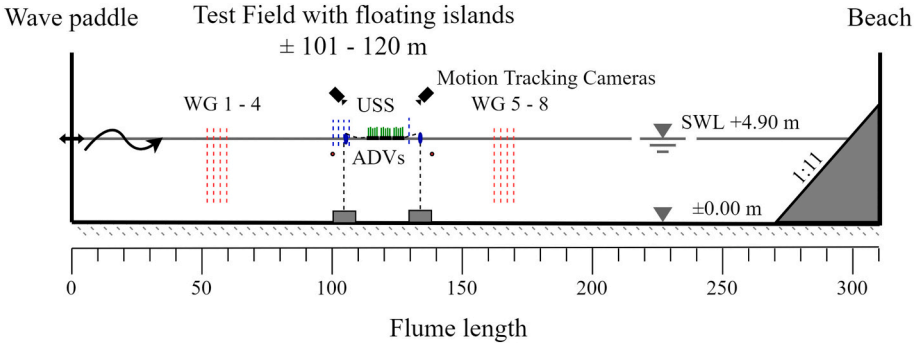

Fig. 1. Large Wave Flume (GWK) with wave paddle to the right, test field with artificial floating islands in the middle and dissipative beach to the right (not to scale). The location of the wave gauges (WGs) needed for the determination of incident and transmitted wave heights alongside the instrumentation in the test field consisting of ultra-sonic sensors (USS), Acoustic Doppler Velocimeters (ADV) and motion tracking cameras are also indicated.

and counter-screwed at four points. The protruding threaded rods on the surface were used for the installation of passive markers for the motion tracking system. During the experiments, the stems of the *Phragmites* were cut approximately 4 cm above the body of the reed gabion to allow for an undisturbed identification of the passive markers. Decay tests for the single reed gabions were carried out to determine their Eigen-frequencies. To this end, a crane was placed over the holding basin, lifting the reed gabions up by 0.20 m and quick releasing them with instrumentation in place. Inertial measurement units were placed in the center of the reed gabion measuring the acceleration of the structure on descend and decay. The gathered data was integrated twice to generate the vertical motion of the structure. The Eigenfrequency of the single reed gabions was determined to be approximately $\omega = 0.93\ s$. Fig. 2 shows the design and fundamental mechanisms of the tested gabions in subpanel (a) and cultivated floating reed gabions in subpanel (b).

2.2. Instrumentation

During the experiments, capacitive wave gauges, ultra-sonic wave gauges, motion tracking cameras and Acoustic Doppler velocimeter (ADV) were used to record the wave parameters as well as the motions of the AFIs.

To measure wave heights, capacitive wave gauges (WG), built in-house, were used. They consist of two electrodes, a measuring wire and a ground plane. Aluminum pipes are used for the electrical grounding to apply a resistance-capacity technique to identify the water surface elevation. Aberrations from the length of the data cable are reduced by the installation of waterproof pre-amplifiers resulting in wave height measurements with accuracies of ±5 mm. The sampling frequency is set to 100 Hz. Two fields of WGs were positioned before and behind the test field. The first WG field, 55 m in front of the AFIs, was installed to obtain surface elevation data for the initial waves. The second WG field, 55 m behind the AFIs, was installed to obtain surface elevation data for the transmitted waves. Locations of the wave gauge fields, between 50 and 60 m and 160–170 m from the wave maker can be seen in Fig. 1.

Furthermore, to measure the free surface water elevation in the vicinity of the AFIs, five ultra-sonic sensors, USS 20130, with the corresponding controller ULS 40-D (General Acoustics, 24,106 Kiel, Germany) were utilized. The accuracy of the sensors is given with 0.36 mm. The sampling frequency is set to 50 Hz. The sensors have a delay of 0.072 s due to internal filtering, which is considered during post processing. Four ultra-sonic sensors (USS 1–4), were positioned inline in front of the structure. The distances between the sensors were determined according to Mansard and Funke (1980) to determine the incident and reflected waves. These sensors, as well as the first wave gauge field, were installed to measure the initial surface elevation and the reflection of structure. Additionally, USS 5 was located 4.5 m behind the floating island to obtain information about the transmitted waves.

To track the motion of the AFIs, four motion-tracking cameras, Oqus 600+ (QUALYSIS, 41105 Gothenburg, Sweden), were installed to the railing of the flume. The cameras send out infrared flashes, which are reflected by the illuminated, passive markers attached to the AFIs. Every single island was outfitted with four markers. The achieved accuracy for calibrated tracking volume is 4 mm in the x-, y- and z-axis. In addition to that, a reference structure was installed in the measurement volume. This stationary L-shaped reference structure with four markers was used to define the origin and orientation of the global coordinate system of the camera system. For the tests, a movement from the wave maker to the dissipative beach corresponds to the x-direction, while a movement

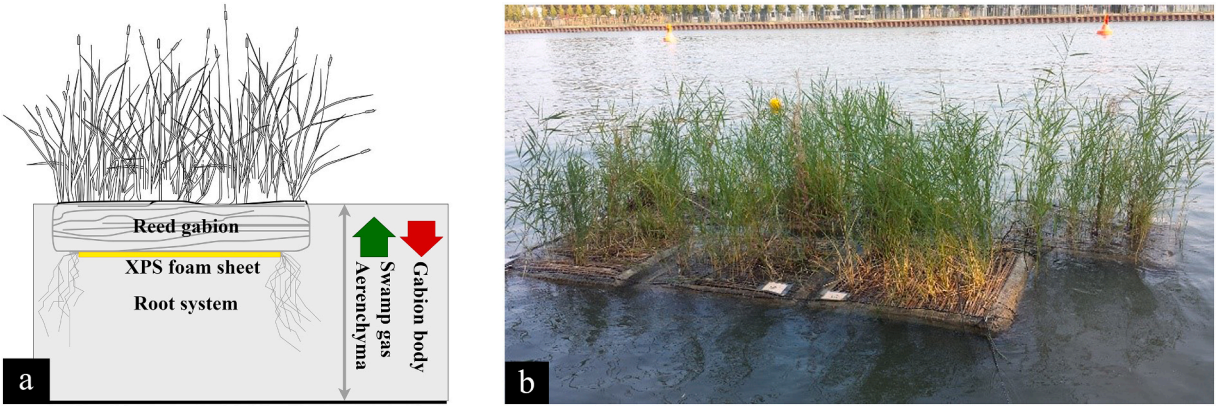

Fig. 2. Sketch of a single reed gabions with added XPS foam sheet and fundamental mechanisms responsible for buoyant behavior (a) and cultivated reed gabions floating in a canal (b).

from the bottom of the flume towards the ceiling describes a movement in the z-direction. The measurement volume covered the whole area of motion of the structure. During wave-structure interaction, the AFIs moved below the still water level.

Two Acoustic Doppler Velocimeter (Nortek, 1351 Rud, Norway) were installed to receive information about the water particle velocity before and behind the structure. The sensors have a maximum sample rate of 200 Hz and an accuracy of the measured value with ±1 mm/s. They employ the Doppler Effect, which enables a contactless three-dimensional velocity measurement in a distance of 5 cm from the transmitter. A first velocimeter was installed on the same x-position as the first USS. The gathered data provides information about the kinematics of the initial waves. A second velocimeter was installed behind the structure to provide information about the kinematic of the transmitted waves. The data from the ADVs will be mainly incorporated in a follow-up manuscript regarding the wave scattering and energy redistribution due to wave-structure interaction. In Fig. 3, the test field with the AFIs and the nearby measurement instruments are shown in a side view.

The experiments were conducted with two different configurations, according to the orientation of the AFIs. The AFIs were installed in a block of 3 × 4 reed gabions and as a block of 4 × 3 gabions, i.e. the length of the structure facing the waves changed between 4 m and 3 m while the width changed between 3 m and 4 m. The first configuration includes three rows of AFIs (3 × 4) while the second configuration has four rows of AFIs (4 × 3) During both sets the AFIs were subjected to 42 combinations of regular waves covering intermediate and deep waters ($0.09 < h/L < 1.4$; h = water depth, L = wavelength). The waves were based on captured time series of water elevations recorded during a preliminary investigation in the Mittellandkanal. Here, the water elevation to the side of the channel was recorded during the passage of cargo and sport vessels. The results from these measurements show that sport boats induce steep secondary waves while cargo vessels mainly induce large primary waves. For both configurations five wave heights were used: 0.10 m, 0.15 m, 0.20 m, 0.25 m, and 0.30 m. Similarly, nine different wave periods were tested: 1.50 s, 1.75 s, 2.00 s, 2.25 s, 2.50 s, 3.00 s, 4.00 s, 6.00 s, and 8.00 s. Due to high wave steepness and limitations of the wave maker some wave parameters combinations could not be tested. The Eigenfrequency of the single reed gabions ($\omega = 0.93\ s$) is lower than the smallest, tested wave period due to limitations of the wave maker. An overview of the tested waves regarding the wave period, wave height, wavelength and steepness can be seen in Table 1.

All tests were conducted at least two times to obtain an appropriate database. Overall, 113 tests with regular waves were conducted. The two configurations of the AFIs are presented in Fig. 4 alongside a photography of the AFIs inside the flume during installation and a clear indication of the width and length of the structure.

2.3. Methodology

For the determination of the overall effectiveness of floating breakwaters the transmission coefficient C_T can be used. Wave transmission describes the phenomenon in which the incident wave energy approaches a floating breakwater at the front side, is dissipated to an extent, and a reduced wave is transmitted at the rear side. The transmission coefficient C_T is determined as:

$$C_T = H_t/H_i \tag{1}$$

Table 1
Test parameter wave large-scale wave tests with artificial, organic floating islands displaying wave periods, –heights, –length and –steepness given.

Wave period [s]	Wave height [m]	Wavelength [m]	Wave steepness [–]
1.5	0.1/0.15/0.2/0.25/0.3/0.35/0.4	3.51	0.028/0.043/0.057/0.071/0.085/0.100/0.114
1.75	0.1/0.15/0.2/0.25/0.3	4.78	0.021/0.031/0.042/0.052/0.063
2.0	0.1/0.15/0.2/0.25	6.24	0.016/0.024/0.032/0.040/0.048
2.25	0.1/0.15/0.2/0.25	7.90	0.013/0.019/0.025/0.032/0.038
2.5	0.1/0.15/0.2/0.25	9.72	0.010/0.015/0.021/0.026/0.031
3.0	0.1/0.15/0.2/0.25/0.3	13.74	0.007/0.011/0.015/0.018/0.022
4.0	0.1/0.15/0.2/0.25/0.3	22.08	0.005/0.007/0.009/0.011/0.014
6.0	0.1/0.15/0.25	37.78	0.003/0.004/0.007
8.0	0.1/0.15/0.25	52.61	0.002/0.003/0.005

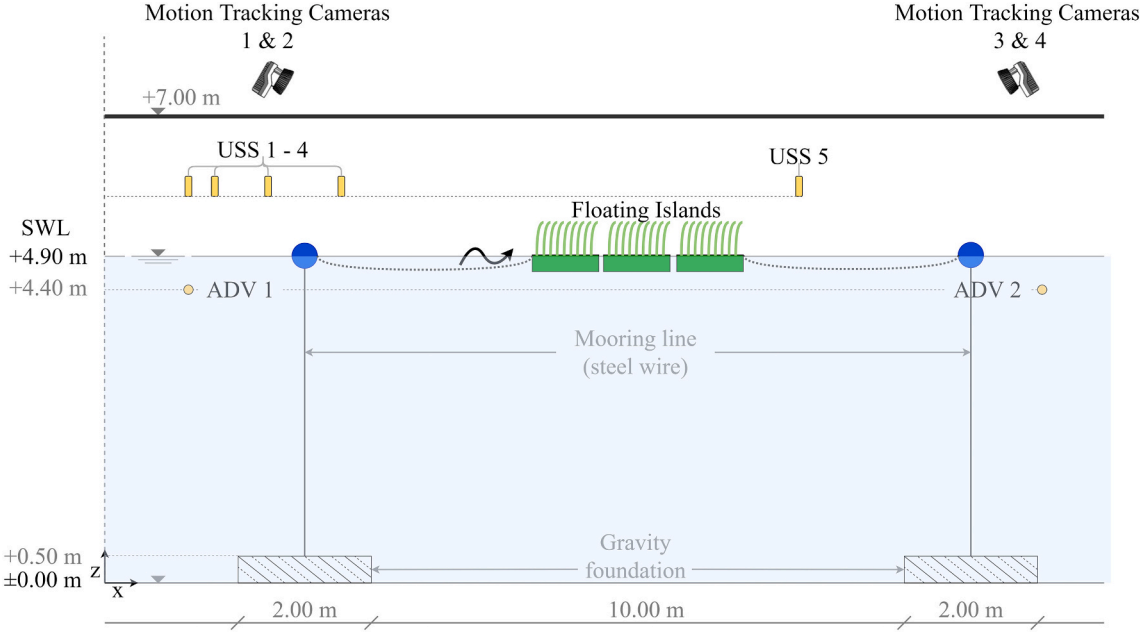

Fig. 3. Instrumentation of the AFI test field with ultra-sonic wave gauges (USS), motion-tracking cameras and Acoustic Doppler Velocimeters (ADV). The artificial floating islands are located in the center with two buoys lifting the mooring line from the ground to minimize their influence on the wave dampening capabilities.

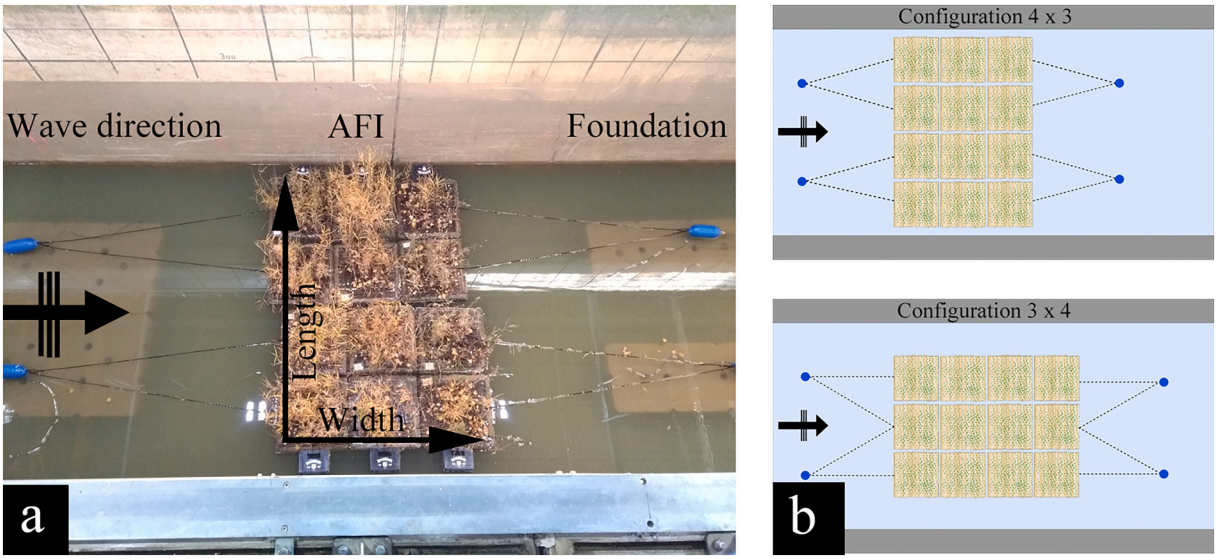

Fig. 4. Large Wave flume during installation with the AFIs, foundation, mooring and buoy system visible (a) and a sketch of the two configurations of AFIs (4 × 3 & 3 × 4) in the flume (b).

with H_t being the transmitted wave height and H_i the initial wave height in meters. The initial wave height is determined using a reflection analysis in the frequency domain based on a method developed by Mansard and Funke (1980), which also leads to the reflection coefficient C_R of the structure. C_R is determined as

$$C_R = H_r/H_i \tag{2}$$

with H_r being the reflected wave height and H_i the initial wave height in meters. By this method, the measured surface elevation is processed to create a time series of the reflected waves. Measurements of the surface elevation at a minimum of two locations with known distance to each other are necessary, which is why the data of the ultrasonic sensors is used. By measuring at multiple locations, different combinations of surface elevations can be compared to obtain a higher reliability regarding the reflection coefficient (Mansard and Funke, 1980). The analysis of the reflection coefficient was carried out in the frequency domain and the phase shifted signals of the measured surface elevation series are determined by the application of a Discrete Fourier Transform (DFT) to approximate the reflection coefficient. This well-established method is based on research by Goda and Suzuki (1976), Mansard and Funke (1980), Frigaard and Brorsen (1995), and Baldock and Simmonds (1999).

C_T is calculated using the data of the wave gauges behind the AFIs for H_t and the resulting H_i from the reflection analysis. Thereby, the measured surface elevation series of the wave gauge needs further pre-processing, than the data of the ultrasonic sensors due to a lower signal to noise ratio. A 2nd order low-pass Butterworth filter is applied. For the identification of relevant data during post-processing, a start time stamp was determined which indicates that the crest height of a measured wave approaches more than half of the ideal wave amplitude height for the following wave crest. This time stamp is shifted to the following crest, to minimize the error of taking a single wave event as start point. The end time stamp of the signal is calculated for a constant number of waves, i.e. 40 waves, as reflected waves from the dissipative beach at the end of the flume are recognizable at the end of the time series. To reduce the influence of reflections for long waves, the relevant wave number N is reduced. The number of cut waves is calculated based on the distance

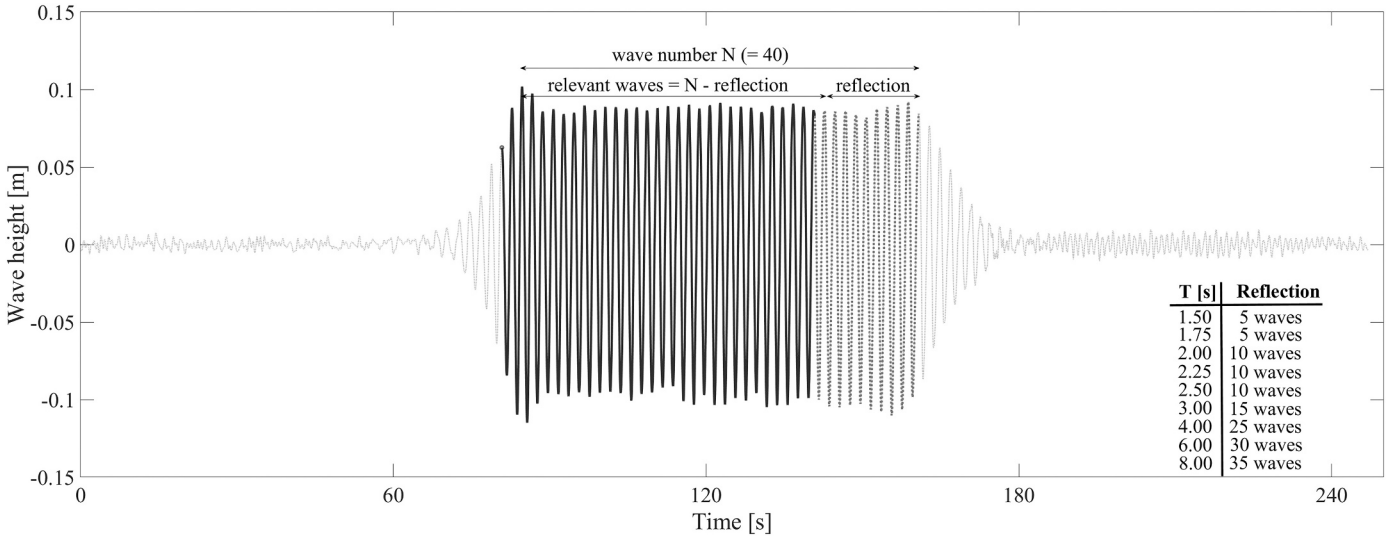

Fig. 5. Identification of relevant data sets with regard to reflection. To obtain the relevant waves the overall wave number N is reduced by the waves were reflections occur. A table depicting the number of cut waves, based on the wave period T, is provided (bottom right).

between the beach and AFIs and the velocity of the corresponding wave. This process is elucidated in Fig. 5 alongside a Table depicting the number of cut waves in regard to the wave period.

The relevant data of initial and transmitted waves is equated in length and compared. The wave periods, wave heights, wavelengths, elevations, velocities, and accelerations for each transmitted and initial wave are calculated with the dispersion relation and 2nd order Stokes equations. The transmission coefficient is calculated for the single initial and transmitted wave height. An example for the creation of the transmission coefficient is shown in Fig. 6.

For the determination of the movement, the passive markers attached to the AFIs are recorded continuously, which results in time series of the spatial coordinates of each AFI. When combined, the spatial coordinates form the trajectories of the AFIs during wave-action. These trajectories include the rotational and translational information, called 6 degrees of freedom (DOF), i.e. the movement in x-, y- and z-direction as well as around each axis over time. The trajectories of all markers located on one gabion are connected to create a rigid body. Every rigid body possess a local coordinate system. A local coordinate system is placed in the geometric center of the reed gabions. The local coordinate systems are referenced within the global coordinate system, which was defined by the L-frame, as described above.

Surge, heave and pitch motion are further analyzed while sway, roll and yaw are considered negligible as no significant motion in these directions was recorded. Surge motion describes the distance covered between the start position of an AFI and the location of maximal horizontal displacement after the test. Heave motion is defined as the movement of an AFI between a wave trough and crest. Pitch motion describes the rotation of the AFI around its geometric center.

3. Results

The identified transmission coefficients are plotted over the wave frequency since a clear dependency on the wave period is expected (see Fig. 7). The results from configurations 1 and 2 are assembled, as the difference in width between both configurations was too small to indicate significant changes in the results. Thus, the data sets of configurations 1 and 2 are merged. This can be seen in Fig. 7 a.

As one main result, Fig. 7 show that waves with low frequencies $f < 0.35\ \left[\frac{1}{s}\right]$ are transmitted almost unaffected. For waves with frequencies of $0.35 < f < 0.50\ \left[\frac{1}{s}\right]$ a reduction of the transmitted wave height of around 10% is observed. For waves with frequencies of $0.50 < f < 0.70\ \left[\frac{1}{s}\right]$ a reduction of the transmitted wave height of up to 50% is observed and the scatter of C_T increases with increasing frequencies. Tests with short waves are less influenced by the reflection of the beach of the wave flume, which is why a higher number of waves was tested. The increasing number of test waves results in a higher statistical deviation. A minimal variation of wave periods caused a scatter of C_T. To reduce this scattering, C_T is plotted against the target wave period set for the test in Fig. 7 b. This approach seems to be reasonable as the wave group with largest scattering (here H = 0.1), reveals that the ideal period is closely positioned to the density distribution of the corresponding data points (cp. Fig. 7 c). Further, medians for all tests with same wave height and same period are calculated and sorted by their wave height along the y-axis for small wave frequencies. The statistical median value was chosen as a descriptor as it is robust against outliers. Outliers present in the data contribute to the large spreading. This is exemplified by the added boxplot for the data of the wave group of H = 0.1 with the largest scattering (cp. Fig. 7 c). The results for the reflection coefficient C_R are plotted over the wave number k [1/m] in Fig. 8. The wave number is defined as $k = \frac{2\pi}{L}$ [1/m] with L being the wavelength. The reflection coefficient C_R has an initial value of 0.1, as reflections in the flume are constantly present due to oblique wave reflections from the tested structure. Waves with $k < 0.8$ [1/m] are not reflected by the structure ($C_R = 0.1$). For waves with $0.8 < k < 1.3$ [1/m] reflections increase to $C_R = 0.2$. For waves with $k > 1.3$ [1/m] a hyperbolic increase of the reflection to $C_R = 0.4$ is observed.

These results are supported by the data from the motion tracking system as displayed in Fig. 9. Here, the motion of a single reed gabion at the center is shown for all the tested wave periods and a wave height of 0.15 m. The variance in heave (z-direction) and surge (x-direction) over time for a single reed gabion at the center of the AFI system is displayed (cp. Fig. 3).

A not-closed orbital motion for wave periods under 2.25 s is visible. The surge motion indicates a transport of the AFIs for short waves, caused by the waves reflecting of the front of the first gabions. This corresponds to the results regarding the reflection and transmission coefficients. For periods below 2.25 s, the surge motion over time increases with decreasing period to a maximum, overall deflection of over 6.0 m. The maximum is reached due to mooring-induced limitations, as the mooring is pulled back with the AFIs. The horizontal movement of the reed gabion is through-dominated for short waves as the high inertia

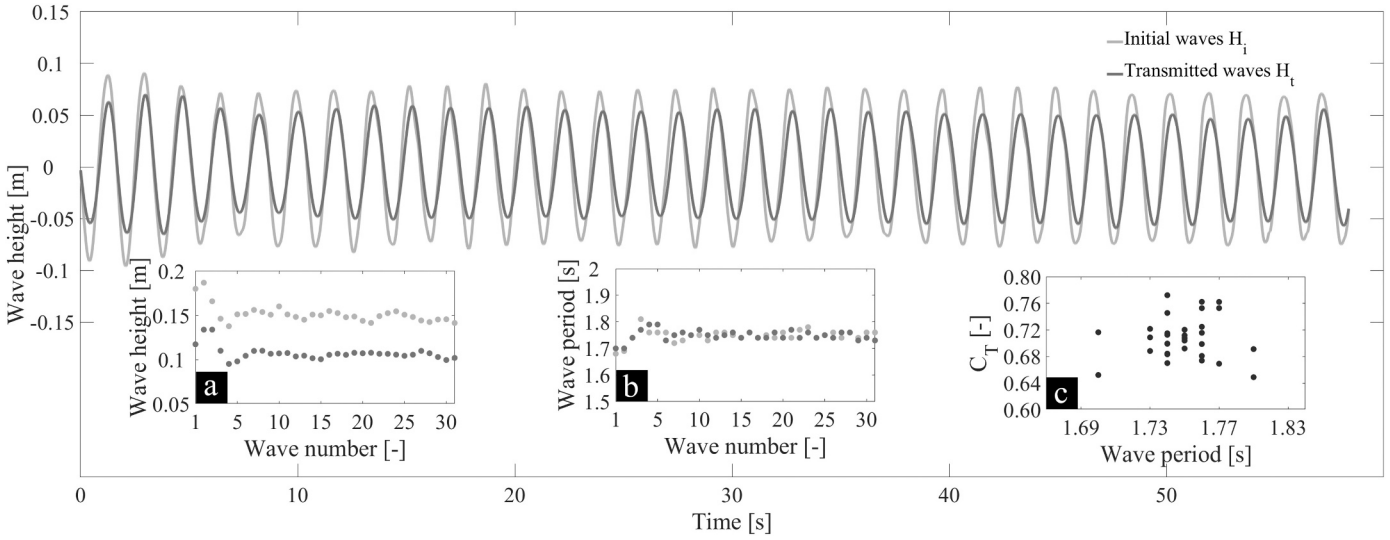

Fig. 6. Exemplary determination of transmission coefficient for a wave with a wave height of H = 0.15 m and wave period of $T = 1.75$ s based on the time series for initial and transmitted wave heights. In the subpanels scatterplots for the wave height (a) and wave period (b) for single initial (light grey) and transmitted (dark grey) waves are shown alongside the resulting transmission coefficients (c).

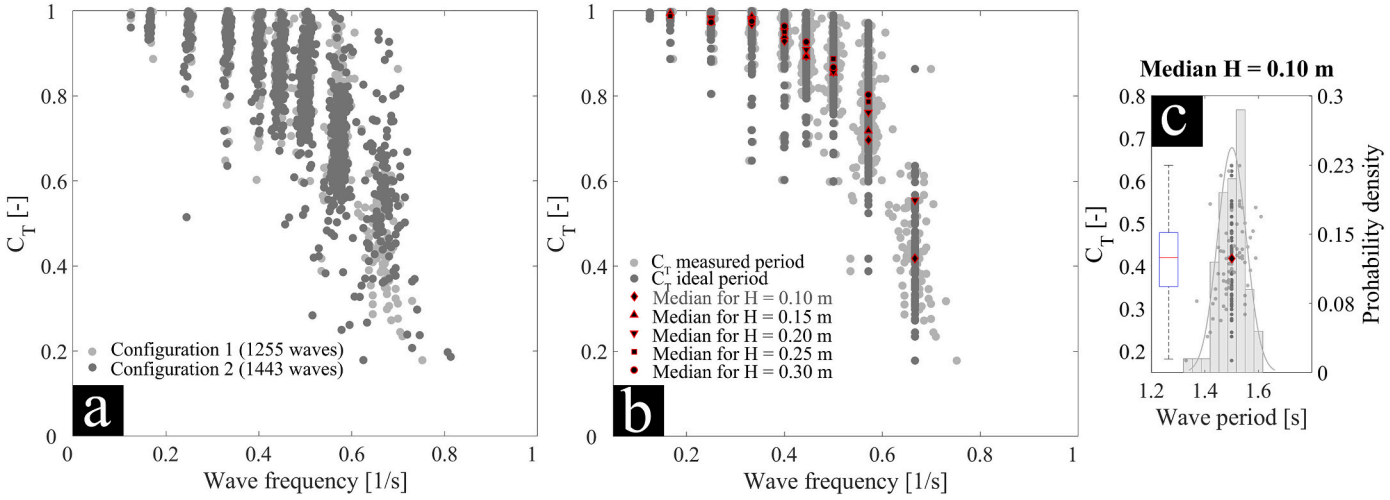

Fig. 7. The transmission coefficient is displayed as a scatter over wave frequency for a composite of configuration 1 (4 × 3 AFIs) and configuration 2 (3 × 4 AFIs) (a). The same data set with medians for tests with varying wave heights is displayed for the measured and ideal wave period (b). A subpanel representation of the distribution for a single wave height, i.e. H = 0.1 m, is given together with the corresponding probability density distribution (c).

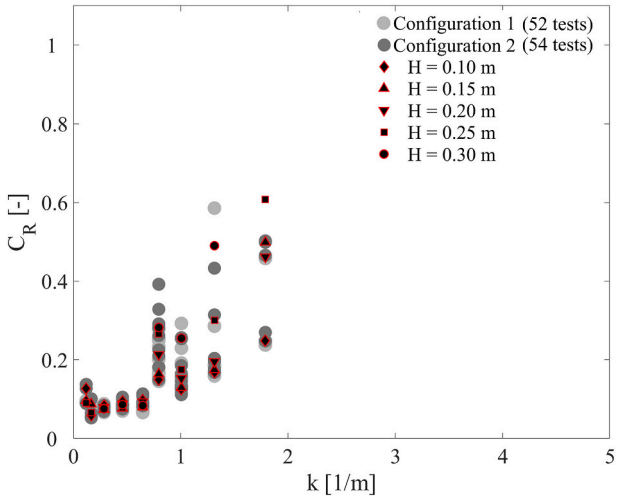

Fig. 8. The reflection coefficient is displayed for a composite of configuration 1 (4 × 3 AFIs) and configuration 2 (3 × 4 AFIs) with the combined medians for tests with varying wave heights displayed for the ideal wave period.

of the AFIs leads to a not-closed orbital motion of the structure. The wave energy is lower than required to fully move the reed gabion with the wave peak. This range of wave periods matches the detected effective range regarding transmission and reflection coefficients. For longer waves with periods of 2.50 s and higher, a full orbital motion of the reed gabion is detected. The wave energy is sufficient to fully or partially lift and transport the reed gabions through the wave orbitals. The elliptical motion for waves with periods of $T > 6.0$ s can be explained by the reflected waves of the beach, which are included in this plot. The reason for the different surge motions of the AFIs is the wave steepness, which is related to the nonlinearity of waves, too. The long wave periods are "intermediate waves", which have a slightly increased (non-linear) wave crest and a longer extended trough than regular sinus waves. Therefore, the longer wave trough increases the time the AFIs are pulled backwards while the waves are passing the AFIs. The short waves below 2.25 s are in deep water conditions with the experimental water depth of 4.9 m. They have a more symmetric or sinusoidal profile but a much higher wave steepness. The higher the wave steepness the higher the loading on the AFI front and the higher the reflected contribution of the wave energy.

4. Discussion

4.1. Wave dissipation

To extrapolate from these results a hyperbolic tangent function is used to fit a curve through the medians of both the transmission and reflection coefficients. The hyperbolic tangent was chosen to include natural boundaries, which exist due to interdependent physical processes influencing the transmission. The resulting functions are further parameterized regarding the dimensionless wave height H/d, with d as the immersion depth of the AFIs (d = 0.25 m). After parameterization, it can be seen, that no influence of the wave height for extremely short and long waves is indicated. This behavior is attributable to the boundary conditions for extremely small and long waves. Concluding, C_T for long waves (k < 0.8) is near 1.0 and thereby all waves are transmitted through the structure. If the waves get shorter (0.8 < k < 3.0) a hyperbolic decrease in C_T is predicted. This means, that other physical processes influence the transmission and waves are no longer transmitted through the structure completely. It is assumed, that extreme short waves k > 3.0 are not transmitted through the structure at all. All in all, it can be said that the influence of wave period for C_T is significant. The influence of wave height for C_T is recognizable but still small in reference to the influence of the wave period. The resulting curves regarding the transmission and reflection coefficient are displayed in Fig. 10, where the extrapolated data is displayed as a dotted line. The coefficient of determination (R^2) as well as the Normalized Root Mean Square Error (NRSME), displayed in the same figure, show a good agreement for the measured part of the graph. The values for the extrapolated data need to be verified in future tests. The data is extrapolated until a wave number of k = 5 [1/m]. The transmission coefficient C_T for k < 0.8 [1/m] is near one, i.e., waves are transmitted with no loss of energy. Similarly, the reflection coefficient C_R is near zero for k < 0.8 [1/m], i.e., waves are not reflected. For 0.8 < k < 3.0 [1/m] the transmission coefficient C_T decreases hyperbolically, i.e. other physical processes, e.g. reflection, influence the transmission and waves are no longer transmitted completely. This is why the reflection coefficient C_R increases for the same wave numbers. Waves with k > 3.0 [1/m] are transmitted to a negligible scale. Reflection for these wave numbers is highly dependent on the H/d-ratio, i.e. the smaller the wave height the more reflection occurs.

Both coefficients show an interactive physical response relating to the wavelength. No reflection and full transmission for long waves (k < 0.8 [1/m]) is recorded as the AFIs move with the water level under

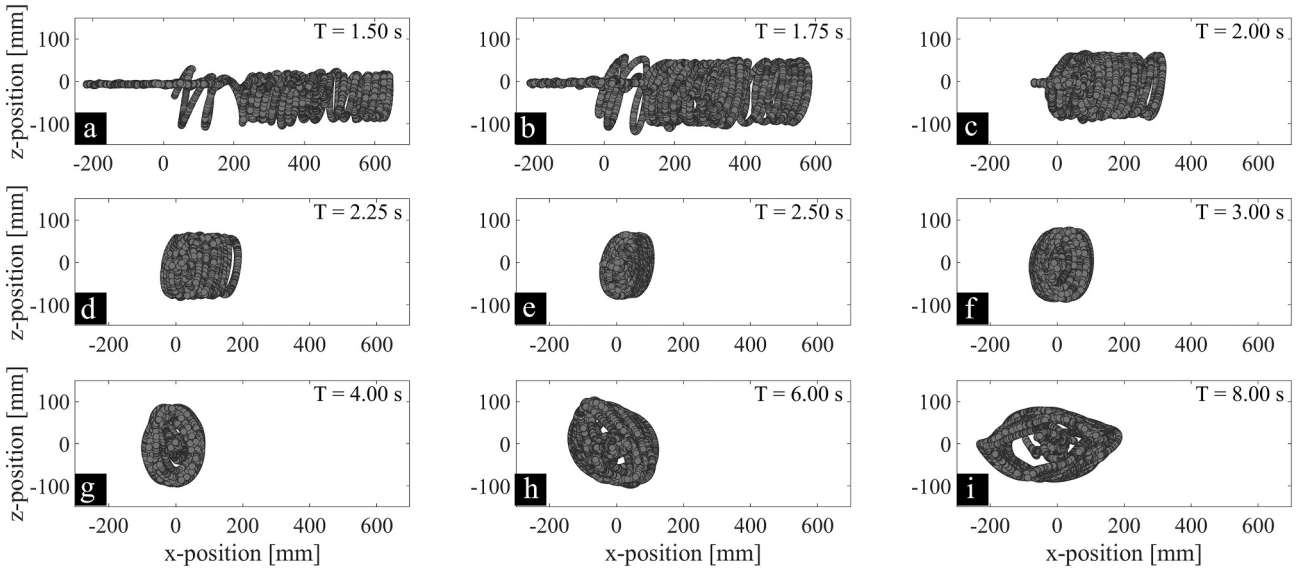

Fig. 9. Motion behavior in heave (z-direction) and the surge (x-direction) over time for a single reed gabion in the center of the AFI. Every subplot (a - i) describes the motion under varying wave periods T = 1.5 s–8.0 s and a constant wave height (H = 0.15 m) for the full test duration.

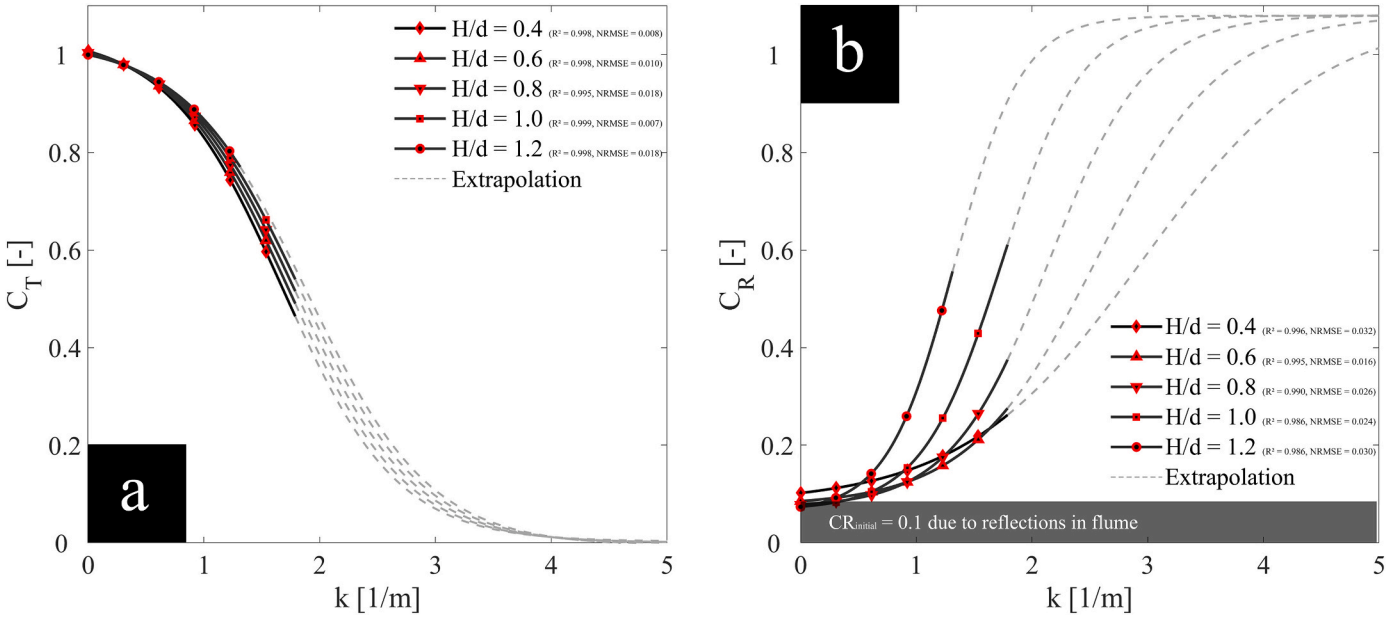

Fig. 10. Results regarding transmission (a) and reflection (b) coefficients, with a distinction regarding the wave height to water depth ratio. The results are extrapolated (dotted line) from the existing data till k = 5. The results show a mirrored behavior of transmission and reflections coefficients for an increasing wave number, i.e. the less waves are transmitted the more reflection and other dissipative processes are involved.

waves. For shorter waves (0.8 < k < 3.0 [1/m]) the difference between the orbital movement of the waves and AFIs, as described above, leads to waves being reflected off the AFIs. Furthermore, the differences in motion between AFI and wave orbital increase the probability of wave breaking and overtopping and therefore lead to a decrease of C_T. Thus, for very short waves (k > 3.0 [1/m]) the reflection approaches a maximum, and the transmission a minimum.

Combining these results, the energy dissipation of the structure can be calculated as:

$$C_{Diss} = \sqrt{1 - C_R^2 - C_T^2} \tag{3}$$

The energy dissipation is calculated for the medians as well as for the extrapolated data and plotted against the wave number, as can be seen in Fig. 11. The maximal energy dissipation of waves can be seen between (1.0 < k < 3.0 [1/m]). Short waves with small wave heights (H/d = 0.4–0.8) are dissipated by up to 85%, while waves with increasing wave heights (H/d = 1.0–1.2) are dissipated by 55–70%. The influence of the wave height is clearly visible as with increasing wave height, i.e., decreasing H/d, the peak dissipation is reduced. The performance of AFIs as a breakwater for secondary ship-induced waves is satisfactory for a width between 4 and 8 m. The energy dissipation between 50 and 85% indicates that the damping performance of the structure depends mainly on the high inertia and surface roughness. The porosity of the structure dissipates small frequencies of oscillating waves and can be interpreted as a natural low pass filter. The damping of longer waves (e.g. primary ship waves) is not as efficient. The energy of long waves exceeds the inertia of the AFIs itself. The structure indicates orbital motions (cp.

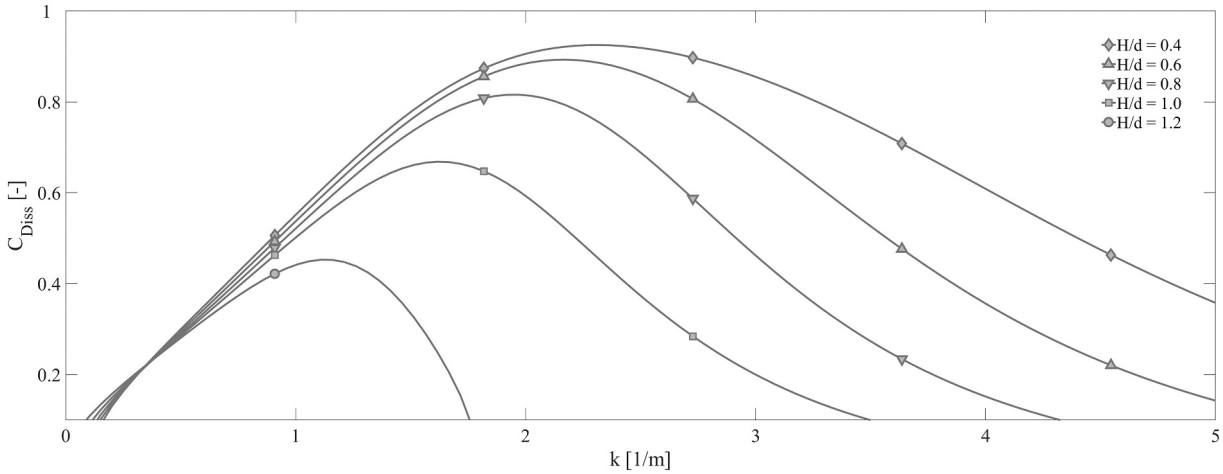

Fig. 11. Predicted dissipation coefficient based on extrapolated data over wave number k with a peak dissipation at $k = 2.5$ for waves with $H/d = 0.4$. With increasing wave height, i.e. decreasing H/d, the peak dissipation is reduced.

Fig. 9 e - f) and therefore no phase shift to the orbital water particle motion. Due to the missing phase shift, no interaction between structure and wave and therefore no significant damping appears.

4.2. System motion

The dissipative behavior of the AFIs can be further explained by taking a closer look at the single dominant motions, i.e. surge, heave, and pitch, presented in Fig. 12. They are displayed for the front, middle and rear reed gabion of the first configuration (3 × 4) over a set number of waves ($n = 50$) for two distinctively different wave periods and wave heights (Setup 1: $T = 1.5$ s, H = 0.10 m; Setup 2: $T = 4.0$ s, H = 0.15 m). The surge motion for the first wave setup in subpanel (a) shows the large lateral displacement of the gabions described above. There are only little differences in the motion between the front, middle, and rear position, as the individual reed gabions are moored together and pushed forward simultaneously. However, the influence of the flexible mooring becomes noticeable. The elastic link used allows for an initial extension until the mooring is activated and the restoring forces slightly pull back the AFIs back towards the wave maker to lessen the impact on the AFIs themselves. This highlights the importance of choosing a fitting mooring, which will in turn affect the effectiveness of the AFIs wave attenuation potential. The second wave setup in subpanel (b) shows that the AFIs are not pushed forward by long waves. For long waves the AFIs indicate an orbital motion, i.e. a motion of the reed gabions with the water particles. This is true for all three positions. The heave motion for the first wave setup in subpanel (c) showcases one of the main wave attenuation properties of the AFIs. A comparison of the vertical motion of the water column and the heave of the AFIs shows that the movement of structure is through-dominated for short waves. The high inertia of the AFIs leads to a not-closed orbital motion of the structure. The wave energy is lower than required to lift the structure on level with the wave peak. While the front reed gabion is nearly fully lifted by the incoming waves are the gabions positioned in the middle and rear lifted far less. This highlights the importance of the structure width for any wave attenuating system. This has been shown in a variety of studies concerning wave dissipation. From offshore aquaculture (Plew et al., 2005; Zhu et al., 2020, 2021) over large floating structures and breakwaters (Zhang et al., 2020) to vegetation and natural phenomena (Lei and Nepf, 2019; Villanueva et al., 2021) it is shown that the width of any marine structure directly affects its ability to attenuate waves. The wider the AFIs are, the better their potential to dampen waves is, as the wave energy necessary to lift the structure as a whole is increased. The heave motion for the second wave setup in subpanel (c) shows that for longer waves with a higher wave energy potential a full orbital motion of the structure is indicated. The pitch motion for the first wave setup, see subpanel (d) does not explicitly indicate a damping behavior. The motion decreases slightly from the front to the rear position. However, a comparison to the longer

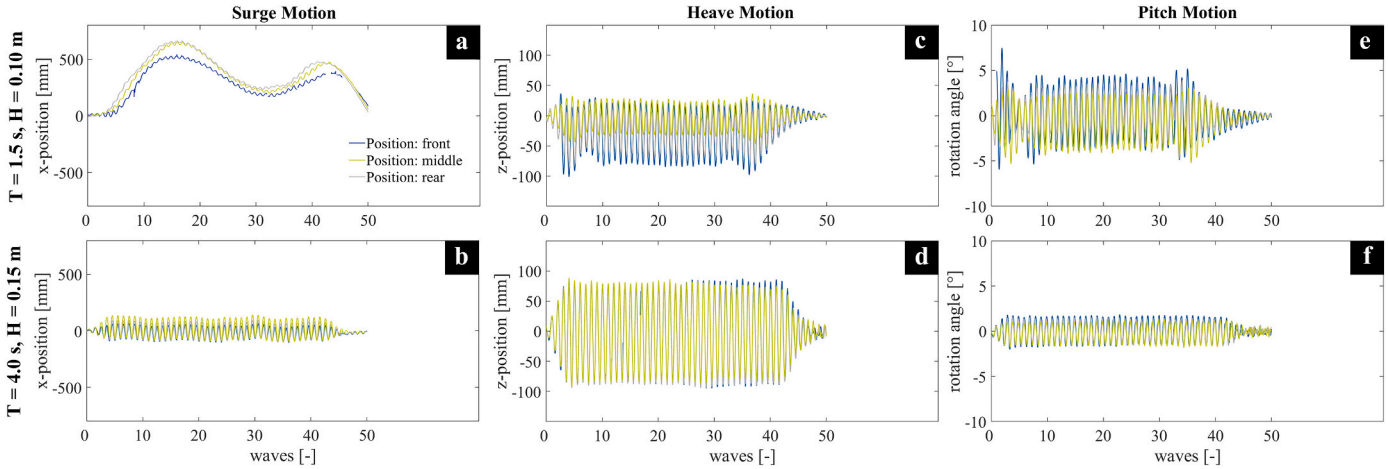

Fig. 12. Surge, heave and pitch motion of front, middle and rear center reed gabion for 50 waves of two wave setups (Setup 1: T = 1.5 s, H = 0.10 m; Setup 2: $T = 4.0$ s, H = 0.15 m).

waves reveals that the rotation angle for the smaller waves is much higher than for the longer waves of the second wave setup (see subpanel (e)). The inertia-influenced motion of the AFIs against the incoming wave leads to this buildup of rotational motion. This might indicate consequences regarding the floating stability of AFIs, which is based on the aerenchyma tissue in the *Phragmites*, which has a lower density than water, and trapped swamp gas, mainly composed of CH4, C02 and N2 (Günther, 2013). It is assumed that the swamp gases escape under high pitch motions. As this was not within the scope of the study, the authors suggest that the effect of pitch motion on the buoyancy needs to be determined in following studies. Based on these results, the authors presuppose that the AFIs are best suited for the attenuation of small to medium wavelengths, e.g. in conditions induced by vessels in a marina or by wind in fetch-limited areas.

4.3. Comparison to traditional, floating breakwaters

To better classify the performance and validate the usefulness of the AFIs in regard to wave dampening the transmission coefficients of other floating breakwater experiments are compared to the results of this study. The results are shown in the subpanels a – f of Fig. 13. Similar floating structures are selected as, to the best of the authors' knowledge, no experimental data regarding the wave dampening capabilities of other AFIs exists. The term "similar" meaning similarity of geometry, i.e. either relative depth $\frac{d}{h}$, with d being the depth of immersion and h the overall water depth or relative length $\frac{W}{L}$, with W being the width of the floating structure normal to the direction of wave propagation and L being the wavelength. This is displayed in Table 2. The efficiency of the AFIs and the floating wave breakers is expressed through the above-mentioned transmission coefficient C_T. It is assumed that the relative length $\frac{W}{L}$, alongside the mass, is the most important parameter as the width is the primary design parameter for any floating breakwater (Peña et al., 2011). The relative length of the tested AFIs ranges from $\frac{W}{L} = 0.05$ to 1.13, while the relative depth is $\frac{d}{h} = 0.05$. In the subpanels of Fig. 13 the range of the relative length is shown to a maximum value of 3.00, as no comparable data exists beyond that point.

Floating tire breakwaters (Giles and Sorensen, 1978) with a relative length of $\frac{W}{L} = 0.16$ to 1.35 and a relative depth of $\frac{d}{h} = 0.19$, which were tested in a wave flume are selected for the comparison. Another floating tire breakwater (Bishop, 1985), with a relative length of $\frac{W}{L} = 0.48$ to 4.92 and a relative depth of $\frac{d}{h} = 0.08$, where recordings were made under field conditions, is selected as well. These floating tire breakwaters are mainly used to provide wave protection at fetch-limited locations with short wave lengths as well as for shoreline erosion control, and for the temporary protection of water-based and coastal operations, e.g., waterfront construction or dredging. A perforated horizontal floating plate breakwater with a relative length of $\frac{W}{L} = 0.13$ to 1.87 and a relative depth of $\frac{d}{h} < 0.37$ (Arunachalam and Raman, 1982) is included in the comparison as it is a light and mobile construction. Based on the concept of energy dissipation through perforations, the floating plate breakwater with perforations on its horizontal plate, was investigated in physical model tests. Another floating breakwater, assembled of a trapezoidal float with and without a submerged row of pipes, investigated in physical experiments is also selected for comparison (Mani, 1991). The relative length of the float ranges from $\frac{W}{L} = 0.08$ to 0.22 and the relative depth is $\frac{d}{h} = 0.16$. With the attached pipes a relative depth of $\frac{d}{h} = 0.46$ is reached. It is shown that the pipe attachment to the trapezoidal float increases the reflection characteristics of the floating breakwater as well as the level of turbulence due to the submerged pipes. This in turn reduces the width requirement for the breakwater. The results of experimental tests of a board-net floating breakwater

Table 2
Overview regarding structural parameters of compared floating breakwaters.

	Study by:	Type of structure:	Relative length $\frac{W}{L}$	Relative depth $\frac{d}{h}$
	Present study	AFI	0.05–1.13	0.05
a	Giles and Sorensen, 1978	Floating tire breakwater	0.16–1.35	0.19
b	Arunachalam and Raman, 1982	Perforated floating plate breakwater	0.13–1.87	0.37
c	Bishop, 1985	Floating tire breakwater	0.48–3.00	0.08
d	Mani, 1991	Trapezoidal breakwater (without pipes)	0.08–0.22	0.16
		(with pipes)		0.46
e	Dong et al., 2008	Board-net floating breakwater	0.82–1.81	0.20
f	Wang and Sun, 2010	Porous floating breakwater	0.13–0.56	0.50

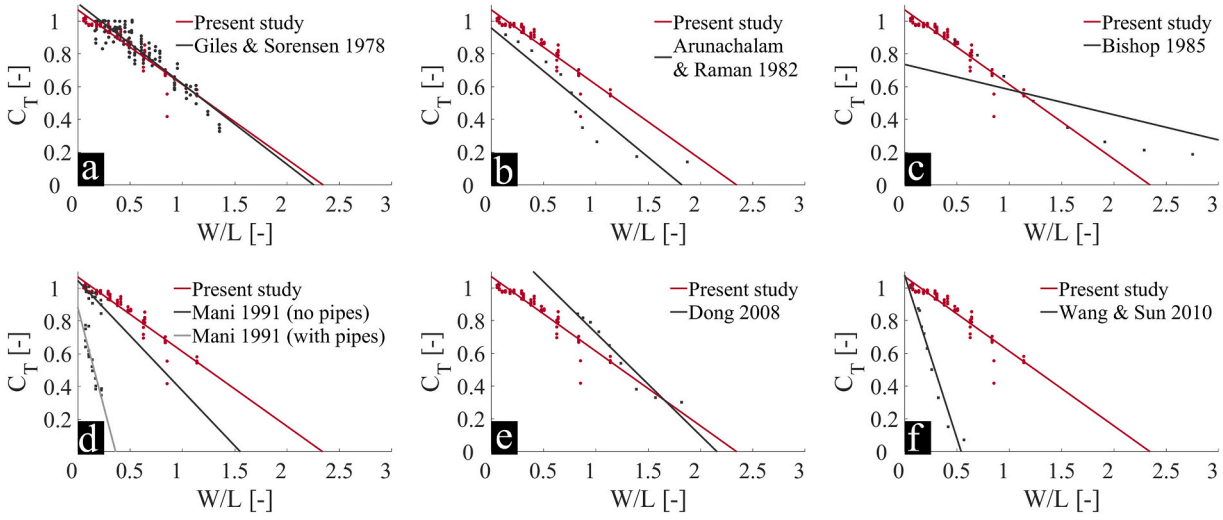

Fig. 13. Comparison of the Transmission coefficient between the studied AFIs and traditional floating breakwaters like floating tire breakwaters (a & c), a perforated horizontal floating plate breakwater (b), a trapezoidal breakwater with and without submerged pipes (d), a board-net floating breakwater (e) and a porous floating breakwater (f). The results are compared in regard to the relative length *W/L*, with *W* being the width of the floating structure normal to the direction of wave propagation and *L* being the wavelength.

consisting of a thin plane board with rows of nets underneath is also chosen for the comparison (Dong et al., 2008). It has a relative length of $\frac{W}{L} = 0.82$ to 1.81 and a relative depth of $\frac{d}{h} = 0.20$. The submerged nets can be compared to the roots of the AFIs. Furthermore, a porous floating breakwater, consisting of perforated diamond-shaped blocks assembled with shafts, with a relative length of $\frac{W}{L} = 0.13$ to 0.56 and a relative depth of $\frac{d}{h} = 0.50$ was used to include porosity of the AFIs as this is also an influential factor (Wang and Sun, 2010). The main parameters of all breakwaters are listed in Table 2.

It is shown, that the AFIs perform similar in comparison to some of the listed floating wave breakers for a comparable relative length, i.e. to the floating tire breakwaters (cp. Fig. 13 a & c), the perforated horizontal floating plate breakwater (cp. Fig. 13 b) and the board-net floating breakwater (cp. Fig. 13 e). This similarity can be explained by the comparable geometry regarding relative length and depth as well as the overall similar dissipation mechanisms used by all wave breakers. According to Dai et al. (2018) and McCartney (1985) these box-type breakwaters, mainly attenuate waves by reflection.

The experiments with large relative depths, i.e. the tests by Mani with pipes attached (1991) (cp. Fig. 13 d) and the porous breakwater tested by Wang and Sun (2010) (cp. Fig. 12 f) indicate that the damping performance increases significantly for short relative lengths. Furthermore, the comparison indicates that the influence of the relative depth is significant. Experiments with large relative depth indicate that the damping performance increases significantly for short relative lengths as a larger draft has a stronger influence on the orbital motion of the water particles. Experiments with low relative depths indicate lower damping capacities for shorter relative wavelengths.

Overall, the comparison shows that the ecologically-preferable AFIs dampen the wave height similar to traditional floating breakwaters and that the wave transmission is mainly a function of the breakwater width to incident wavelength ratio with a dependence on the relative depth and the dissipation mechanism targeted by the individual system.

4.4. Influential parameters

The comparison of the studies shows, that the overall effectiveness of the AFIs and floating breakwaters depends on a variety of hydrodynamic, mechanical, as well as biological parameters. Fig. 14 illustrates the major components of the studied system and gives an overview of the interacting mechanisms, which influence the wave damping performance.

The roots of the AFIs act as aquatic suspended canopies, i.e. porous obstacles that are suspended from the water surface with a gap between the canopy and the bottom of the water where biological processes, such as the decomposition of plant matter lead to entrapped gas and positive buoyancy. These suspended canopies are known to increase the flow resistance while simultaneously reducing the flow speed within the root system. As shown by a number of studies, suspended canopies alter the ambient flow and thus decrease current speeds and directions within and below the canopy (Blanco et al., 1996; Plew et al., 2005). The effect has especially been observed in regard to net-based and longline aquaculture (Bi et al., 2015; Zhao et al., 2013, 2015; Zhu et al., 2021) which present a promising option to also attenuate waves apart from providing a sustainable source of nutrition. The effect of the submerged canopies is also dependent on the density of the root system, as it increases the effective depth of immersion and the inertial force due to the enclosed water within the water column, which acts as added mass to the AFIs. Generally, the consideration of the suspended root system further reduces the wave height due to increased drag forces and amplified wake formations around the structure, which effects the velocity profile. Similar to emergent canopies, wave attenuation is affected by the vegetation. Rupprecht et al. (2017) showed that the contribution of vegetation to wave dissipation is plant species specific, i.e. in this study the rigidity and density of the root system would affect flow conditions. This indicates that an inclusion of the submerged canopies provides further wave dampening potential for AFIs.

Moreover, the trapped swamp gas in the canopy supports the buoyancy of the AFIs. The retention of the swamp gas under waves is a critical step towards the successful implementation of fully organic AFIs. Further studies including controlled gas pockets under the gabions are subject to ongoing research, to quantify the displaced gas due to waves as indicator which wave profiles can be effectively dampened over time. The time depending performance is used to evaluate the number of impacting waves, i.e. connected to passing ships, and the recovering time of buoyancy forces. Subsequently, this leads to the longevity of fully organic AFIs under waves. Furthermore, the inclusion of buoyant polymer foams as substrate material for AFIs could enhance said

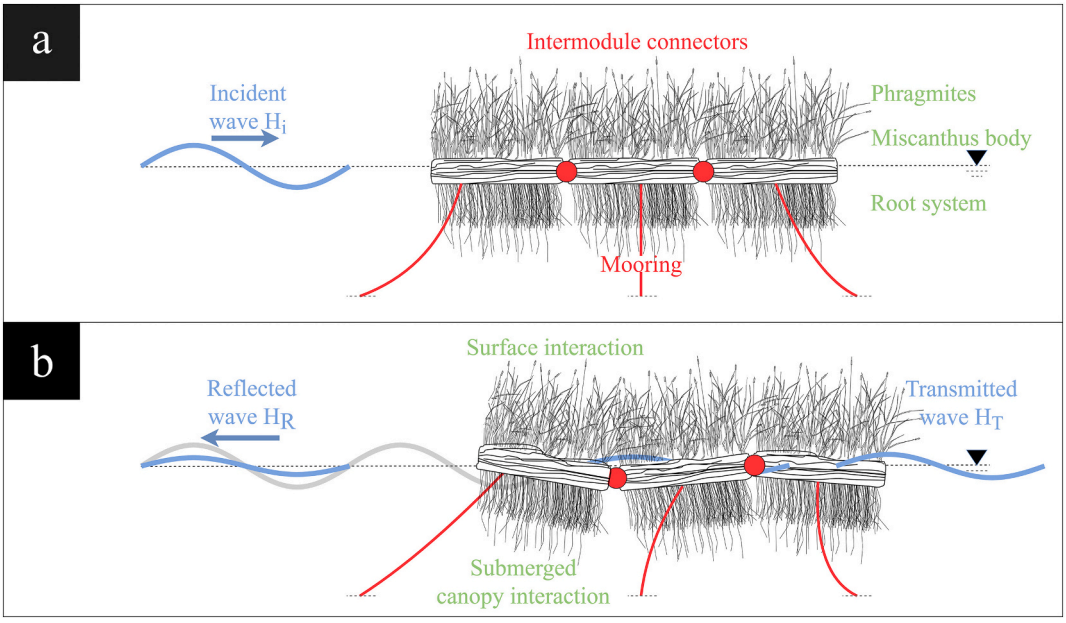

Fig. 14. The incident wave (a) is shown alongside the reflected and transmitted wave as well as the major mechanical components influencing the wave dampening performance of the AFIs under wave action (b), such as the mooring line, inter-module connectors, the Phragmites covered surface area, and the submerged roots.

longevity (Dahl, 1972). In this study, XPS-panels were used to simulate the swamp gas to allow for constant testing conditions and to investigate critical wave conditions with regard to the sea-keeping characteristics and wave dissipation performance. Future research will focus on the effect of the AFIs without the XPS-panels, and the effect of the suspended root system.

The mooring design, arrangement and configuration directly affect the motion behavior and sea-keeping characteristics of the AFIs. The elastic mooring for the tests of this study was designed to allow drift motions within a certain range (approximately 3 m) of the AFIs starting position, to investigate the wave damping performance of the AFIs itself. The same elastic link was used for the intermodule connector. The low mooring stiffness allows for a swing motion between the gabions, which keeps the anchoring forces lower and thus the external influence on the gabion system. The intermodule connectors between single AFI elements also has a large influence on the hydrodynamic response of the whole system. According to Diamantoulaki and Angelides (2010), the configuration of an breakwater array connected with hinges strongly affects the hydrodynamic response and the effectiveness of a breakwater arrangement. The combination of the elastic horizontal mooring system and the elastic intermodule connections used in the present study has an effect on the reflection coefficient and dampening capability of the AFIs. The flexible mooring system generates restoring forces, equivalent to the spring stiffness and length of the mooring lines. The short lengths of intermodule mooring connectors enable only small displacements between the single rows of AFIs. This means, that especially the second row of AFIs is forced back by the first row of AFIs and generates reflected waves like a fixed system. Thereby, it is not necessary that the global system is maximally displaced to activate the restoring forces in the intermodule connections. This effect increases the efficiency of the structure while ensuring flexibility against failure of intermodule connectors. The increased reflection by induced restoring forces of intermodule mooring lines could also explain differences to the small reflection coefficients of tests with flexible floating breakwaters. A higher mooring stiffness would increase the wave dampening performance; however, this would be primarily due to the mooring system and not because of a better performance of the AFIs themselves. This needs to be considered during the design stage to optimize the wave dampening potential and minimize stresses on the mooring. A study by Zhao et al. (2015) suggests that the stresses exerted on upstream anchors will likely be highest and increase with the size of the configuration. The arrangement and configuration has an effect on the flow velocity, as was shown in a comparable, numerical study by Zhao et al. (2013). They showed the distribution of flow velocity at different spacing distances between net cages used in aquaculture as well as with varying numbers of net cages. Their results suggest that especially the number of cages installed in line has an effect on the flow reduction. This fits to the observation that longer structure widths of breakwaters or AFIs lead to a higher damping of incoming waves. As the number of AFIs increases, the wave transmission coefficient downstream from the AFIs will likely decrease gradually because of the increasing damping effect. This needs to be considered similarly during the design and shows that the mooring design contributes significantly to the behavior and damping performance of AFIs and floating breakwaters in general.

In the case of a system failure of the AFIs, e.g. through a collision with a vessel, the floating islands are designed with their failure in mind. Thus, the AFIs introduced to the waters are thought to be ecologically and operationally safe upon failure. The reeds used in the gabions consist mainly of common reed (*P. australis*), native to the African and Eurasian continents and can easily be substituted with endemic plants worldwide. Thus, the ecological impact upon failure can be seen as negligible. The wire mesh currently used for stabilization can be retrieved after a failure. For the fully developed AFIs a biodegradable, recyclable wire solution is planned. That would further eliminate anthropogenic products from the AFIs and minimalize possible health and environmental risks.

5. Conclusions and recommendations

In the present study, the hydrodynamic interaction of regular waves and AFIs, which are based on the secondary wave system of vessels, are investigated. Physical model tests were conducted in a large-scale facility and following results are concluded:

- a comprehensive analysis of the hydrodynamic interaction of waves and AFIs show a significant damping performance of the investigated AFIs for wave periods $T \leq 2.25$ s (cp. Fig. 10). The transmitted wave height of the incident waves is reduced by 50% for the smallest wave periods $T \leq 1.5$ s. The incident waves are reflected between 20 and 50% for these wave periods. The incident wave energy is dissipated by up to 85% for the smallest wave height and period (H = 0.10 m, T = 1.5 s) (cp. Fig. 11). The damping performance of the structure depends mainly on the submerged depth, width, and mass of the AFIs.
- the results regarding transmission, reflection and dissipation need to be seen in connection with the hydrodynamic motion of the structure (cp. Fig. 9). It was shown that waves with long periods, comparable to the primary wave system of a passing vessel, lead to orbital motions of the AFIs and no significant damping. Waves with shorter periods, comparable to the secondary wave system of a passing vessel, describe not-closed orbital motions as the wave energy does not exceed the inertia of the structure and this in turn leads to wave damping. Overall, the performance of AFIs as floating breakwaters for vessel induced secondary wave systems can be seen as satisfactory.

This study takes a first step in predicting the effectiveness of AFIs as floating breakwaters. Based on these findings researchers, industry and government officials alike are enabled to better evaluate AFIs regarding their value for the protection of the shoreline and the ecosystem. AFIs are an appealing addition to existing revetment options, as they do not require additional land use and offer a variety of ecosystem services. In the context of the EU Water Framework Directive (2000) (European Commission, 2000), the AFIs could help to achieve a "*good ecological status*" of waterways as they are expected to lessen the morphological damage due to shipping, increase water quality and serve as an ecological stepping-stone. In the future, numerical or physical investigations are needed to determine the influence of the arrangement and configuration of the AFIs themselves, of the root system, of the wave scattering and energy redistribution due to wave-structure interaction, and of the mooring.

Glossary

Symbol	Appellation (Dimension)
AFI	Artificial Floating Islands (–)
DOF	Degree of freedom (–)
C_{Diss}	Dissipation coefficient (–)
ω	Eigenfrequency (s)
XPS	Extruded polystyrene (–)
f	Frequency (s^{-1})
H_i	Initial wave height (m)
H_r	Reflected wave height (m)
C_R	Reflection coefficient (–)
W	Structure width (m)
d	Submergence depth (m)
C_T	Transmission coefficient (–)
H_t	Transmitted wave height (m)
USS	Ultra-sonic sensor (–)
h	Water depth (m)
WG	Wave gauge (–)
H	Wave height (m)
k	Wave number (m^{-1})

T Wave period (s)
L Wavelength (m)

CRediT authorship contribution statement

Jannis Landmann: Conceptualization, Methodology, Writing – original draft, Writing – review & editing. **Tim C. Hammer:** Conceptualization, Methodology, Writing – review & editing. **Henning Günther:** Writing – review & editing. **Arndt Hildebrandt:** Conceptualization, Funding acquisition, Writing – review & editing, Supervision.

Declaration of Competing Interest

The authors declare that they have no known competing financial interests or personal relationships that could have appeared to influence the work reported in this paper.

Acknowledgments

The presented analyses are embedded in the investigations of the project "*33496/01 - "BioSchWelle": Erprobung der Wellendämpfung durch „lebende Inseln" zur Erhöhung der Artenvielfalt in Gewässern*", funded by the Deutsche Bundesstiftung Umwelt (DBU). The authors thank the staff of the GWK for their support during the preparation of the experiments as well as during the tests.

References

Adee, B.H., 1974. Analysis of floating breakwater mooring forces. Ocean Eng. Mech. 1 (1), 77–92.
Adee, B.H., 1975. Analysis of floating breakwater performance. In: PROC. 2ND. Annu. SYMP. Waterw. HARBOURS Coast. ENGNG. DIV. ASCE Model. Tech., pp. 1585–1602.
Adee, B.H., 1976. Floating breakwater performance. In: Proc. 15th Conf. Coast. Eng., pp. 2777–2791.
Arunachalam, V.M., Raman, H., 1982. Experimental studies on a perforated horizontal floating plate breakwater. Ocean Eng. 9 (1), 35–45.
Baldock, T.E., Simmonds, D.J., 1999. Separation of incident and reflected waves over sloping bathymetry. Coast. Eng. 38 (3), 167–176. Elsevier. https://doi.org/10.1016/S0378-3839(99)00046-0.
Barco, A., Borin, M., 2020. Treatment performances of floating wetlands: a decade of studies in North Italy. Ecol. Eng. 158, 106016. Elsevier B.V. https://doi.org/10.1016/j.ecoleng.2020.106016.
Bi, C.W., Zhao, Y.P., Dong, G.H., Cui, Y., Gui, F.K., 2015. Experimental and numerical investigation on the damping effect of net cages in waves. J. Fluids Struct. 55, 122–138. Academic Press. https://doi.org/10.1016/j.jfluidstructs.2015.02.010.
Bishop, C.T., 1985. Field assessment of floating tire breakwater. Can. J. Civ. Eng. 12, 782–795. https://doi.org/10.1139/l85-092.
Blanco, J., Zapata, M., Moroño, Á., 1996. Some aspects of the water flow through mussel rafts. Sci. Mar. 60 (2–3), 275–282.
Chang, N., Bin, K., Islam, Z. Marimon, Wanielista, M.P., 2012. Assessing biological and chemical signatures related to nutrient removal by floating islands in stormwater mesocosms. Chemosphere 88 (6), 736–743. Elsevier Ltd. https://doi.org/10.1016/j.chemosphere.2012.04.030.
Dahl, H.J., 1972. Untersuchung von Pflanzenarten Auf Ihre Eignung Zum Bau Schwimmender Pflanzeninseln (German). Leibniz Universität Hannover.
Dai, J., Wang, C.M., Utsunomiya, T., Duan, W., 2018. Review of recent research and developments on floating breakwaters. Ocean Eng. 158 (October 2017), 132–151. Elsevier Ltd. https://doi.org/10.1016/j.oceaneng.2018.03.083.
Diamantoulaki, I., Angelides, D.C., 2010. Analysis of performance of hinged floating breakwaters. Eng. Struct. 32 (8), 2407–2423. Elsevier Ltd. https://doi.org/10.1016/j.engstruct.2010.04.015.
Dong, G.H.H., Zheng, Y.N.N., Li, Y.C.C., Teng, B., Guan, C.T.T., Lin, D.F.F., 2008. Experiments on wave transmission coefficients of floating breakwaters. Ocean Eng. 35 (8–9), 931–938. Pergamon. https://doi.org/10.1016/j.oceaneng.2008.01.010.
Eller, F., Skálová, H., Caplan, J.S., Bhattarai, G.P., Burger, M.K., Cronin, J.T., Guo, W.-Y., Guo, X., Hazelton, E.L.G., Kettenring, K.M., Lambertini, C., McCormick, M.K., Meyerson, L.A., Mozdzer, T.J., Pyšek, P., Sorrell, B.K., Whigham, D.F., Brix, H., 2017. Cosmopolitan species as models for ecophysiological responses to global change: the common reed phragmites australis. Front. Plant Sci. 8 (November) https://doi.org/10.3389/fpls.2017.01833.
Engloner, A.I., 2009. Structure, growth dynamics and biomass of reed (*Phragmites australis*) – A review. Flora - Morphol. Distrib. Funct. Ecol. Plants 204 (5), 331–346. https://doi.org/10.1016/j.flora.2008.05.001.
European Commission, 2000. Directive 2000/60/EC of the European Parliament and of the Council of 23 October 2000 establishing a framework for Community action in the field of water policy. Off. J. Eur. Communities 0001–0073.
Frigaard, P., Brorsen, M., 1995. A time-domain method for separating incident and reflected irregular waves. Coast. Eng. 24 (3–4), 205–215. https://doi.org/10.1016/0378-3839(94)00035-V.
Gabel, F., Lorenz, S., Stoll, S., 2017. Effects of ship-induced waves on aquatic ecosystems. Sci. Total Environ. 601–602, 926–939. Elsevier B.V. https://doi.org/10.1016/j.scitotenv.2017.05.206.
Giles, M.L., Sorensen, R.M., 1978. Prototype Scale Mooring Load and Transmission Tests for a Floating Tire Breakwater. Coastal Engineering Research Cente (U.S.), Fort Belvoir, USA.
Goda, Y., Suzuki, Y., 1976. Estimation of incident and reflected waves in random wave experiments. Coast. Eng. 1976 828–845. Proceedings.
Günther, H., 2013. Lebende Inseln Selbstschwimmende Pflanzengesellschaften für Urbane Gewässer. Technischen Universität Berlin.
Headley, T.R., Tanner, C.C., 2012. Constructed wetlands with floating emergent macrophytes: an innovative stormwater treatment technology. Crit. Rev. Environ. Sci. Technol. 42 (21), 2261–2310. https://doi.org/10.1080/10643389.2011.574108.
Hogg, E.H., Wein, R.W., 1988. The Contribution of Typha Components to floating Mat Buoyancy. Ecology 69 (4), 1025–1031.
Hubbard, R.K., 2010. Floating vegetated mats for improving surface water quality. In: Shah, V. (Ed.), Emerg. Environ. Technol., vol. II Springer Netherlands, Dordrecht, pp. 211–244.
Kadlec, R.H., Bevis, F.B., 2009. Wastewater treatment at the Houghton Lake wetland: Vegetation response. Ecol. Eng. 35 (9), 1312–1332. https://doi.org/10.1016/j.ecoleng.2008.11.001.
Kadlec, R.H., Wallace, S.D., 2009. Treatment Wetlands. Treat. Wetl. CRC Press Taylor & Francis Group.
Kaul, R.B., 1974. Ontogeny of Foliar Diaphragms in Typha Latifolia. Am. J. Bot. 61 (3), 318–323.
Lei, J., Nepf, H., 2019. Wave damping by flexible vegetation: connecting individual blade dynamics to the meadow scale. Coast. Eng. 147, 138–148. Elsevier B.V. https://doi.org/10.1016/j.coastaleng.2019.01.008.
Loukogeorgaki, E., Yagci, O., Sedat Kabdasli, M., 2014. 3D Experimental investigation of the structural response and the effectiveness of a moored floating breakwater with flexibly connected modules. Coast. Eng. 91, 164–180. https://doi.org/10.1016/j.coastaleng.2014.05.008.
Ma, C., Qiao, Y., Bin, L., Yao, Y., 2021. Performance of hybrid-constructed floating treatment wetlands in purifying urban river water: a field study. Ecol. Eng. 171, 106372. Elsevier B.V. https://doi.org/10.1016/j.ecoleng.2021.106372.
Machado Xavier, M.L., Janzen, J.G., Nepf, H., 2018. Numerical modeling study to compare the nutrient removal potential of different floating treatment island configurations in a stormwater pond. Ecol. Eng. 111 (July 2017), 78–84. Elsevier. https://doi.org/10.1016/j.ecoleng.2017.11.022.
Mani, J.S., 1991. Design of Y-frame floating breakwater. J. Waterw. Port Coast. Ocean Eng. 117 (2), 105–119. https://doi.org/10.1061/(ASCE)0733-950X(1991)117:2(105).
Mansard, E.P.D., Funke, E.R., 1980. The measurement of incident and reflected spectra using a least squares method. Coast. Eng. 154–172. https://doi.org/10.1061/9780872622647.008.
Marzec, M., Jóźwiakowski, K., Dębska, A., Gizińska-Górna, M., Pytka-Woszczyło, A., Kowalczyk-Juśko, A., Listosz, A., 2018. The efficiency and reliability of pollutant removal in a hybrid constructed wetland with common reed, Manna Grass, and Virginia mallow. Water 10 (10), 1445. https://doi.org/10.3390/w10101445.
McCartney, B.L., 1985. Floating breakwater design. J. Waterw. Port Coast. Ocean Eng. 111 (2), 304–318. https://doi.org/10.1061/(ASCE)0733-950X(1985)111:2(304).
Nakamura, K., Mueller, G., 2008. Review of the performance of the artificial floating island as a restoration tool for aquatic enviro nments. In: World Environ. Water Resour. Congr. American Society of Civil Engineers, Honolulu, Hawaii, United States.
Peña, E., Ferreras, J., Sanchez-Tembleque, F., 2011. Experimental study on wave transmission coefficient, mooring lines and module connector forces with different designs of floating breakwaters. Ocean Eng. 38 (10), 1150–1160. https://doi.org/10.1016/j.oceaneng.2011.05.005.
Plew, D.R., Stevens, C.L., Spigel, R.H., Hartstein, N.D., 2005. Hydrodynamic implications of large offshore mussel farms. IEEE J. Ocean. Eng. 30 (1), 95–108. https://doi.org/10.1109/JOE.2004.841387.
Rahman, M.A., Mizutani, N., Kawasaki, K., 2006. Numerical modeling of dynamic responses and mooring forces of submerged floating breakwater. Coast. Eng. 53 (10), 799–815. https://doi.org/10.1016/j.coastaleng.2006.04.001.
Rupprecht, F., Möller, I., Paul, M., Kudella, M., Spencer, T., van Wesenbeeck, B.K., Wolters, G., Jensen, K., Bouma, T.J., Miranda-Lange, M., Schimmels, S., 2017. Vegetation-wave interactions in salt marshes under storm surge conditions. Ecol. Eng. 100, 301–315. Elsevier B.V. https://doi.org/10.1016/j.ecoleng.2016.12.030.
Saviolo Osti, J.A., Carmo, Do C.F., Cerqueira, M.A. Silva, Giamas, M.T. Duarte, Peixoto, A.C., Vaz-dos-Santos, A.M., Mercante, C.T.J., 2020. Nitrogen and phosphorus removal from fish farming effluents using artificial floating islands colonized by *Eichhornia crassipes*. Aquac. Rep. 17 (April), 100324. Elsevier B.V. https://doi.org/10.1016/j.aqrep.2020.100324.
Sawaragi, T., 1995. Coastal engineering - waves, beaches, wave-structure interactions. In: Coast. Eng. - waves, beaches, wave-structure Interact.
Shealer, D.A., Buzzell, J.M., Heiar, J.P., 2006. Effect of floating nest platforms on the breeding performance of Black Terns. J. F. Ornithol. 77 (2), 184–194. Blackwell Publishing Inc. https://doi.org/10.1111/j.1557-9263.2006.00040.x.

Silinski, A., Heuner, M., Schoelynck, J., Puijalon, S., Schröder, U., Fuchs, E., Troch, P., Bouma, T.J., Meire, P., Temmerman, S., 2015. Effects of wind waves versus ship waves on tidal marsh plants: a flume study on different life stages of scirpus maritimus. PLoS One 10 (3), 1–16. Public Library of Science. https://doi.org/10.1371/journal.pone.0118687.

Soukup, A., Votrubova, O., Cizkova, H., 2002. Development of anatomical structure of roots of Phragmites australis. New Phytol. 153 (2), 277–287. https://doi.org/10.1046/j.0028-646X.2001.00317.x.

Villanueva, R., Thom, M., Visscher, J., Paul, M., Schlurmann, T., 2021. Wake length of an artificial seagrass meadow: a study of shelter and its feasibility for restoration. J. Ecohydraul. 1–15. https://doi.org/10.1080/24705357.2021.1938256.

Vymazal, J., Zhao, Y., Mander, Ü., 2021. Recent research challenges in constructed wetlands for wastewater treatment: a review. Ecol. Eng. 169, 106318. Elsevier B.V. https://doi.org/10.1016/j.ecoleng.2021.106318.

Wang, H.Y., Sun, Z.C., 2010. Experimental study of a porous floating breakwater. Ocean Eng. 37 (5–6), 520–527. https://doi.org/10.1016/j.oceaneng.2009.12.005.

Ware, J., Callaway, R., 2019. Public perception of coastal habitat loss and habitat creation using artificial floating islands in the UK. PLoS One 14 (10). https://doi.org/10.1371/journal.pone.0224424. K. A. Dafforn, ed.. e0224424.

Williams, A.N., Lee, H.S., Huang, Z., 2000. Floating pontoon breakwaters. Ocean Eng. 27 (3), 221–240. Elsevier Science Ltd. https://doi.org/10.1016/S0029-8018(98)00056-0.

Xiang, Y., Fu, Z. Min, Meng, Y., Zhang, K., Cheng, Z. Fei, 2019. Analysis of wave clipping effects of plain reservoir artificial islands based on MIKE21 SW model. Water Sci. Eng. 12 (3), 179–187. Elsevier. https://doi.org/10.1016/J.WSE.2019.08.002.

Zhang, H., Zhou, B., Vogel, C., Willden, R., Zang, J., Zhang, L., 2020. Hydrodynamic performance of a floating breakwater as an oscillating-buoy type wave energy converter. Appl. Energy 257, 113996. Elsevier. https://doi.org/10.1016/J.APENERGY.2019.113996.

Zhao, Y.P., Bi, C.W., Dong, G.H., Gui, F.K., Cui, Y., Xu, T.J., 2013. Numerical simulation of the flow field inside and around gravity cages. Aquac. Eng. 52, 1–13. https://doi.org/10.1016/j.aquaeng.2012.06.001.

Zhao, Y.P., Bi, C.W., Chen, C.P., Li, Y.C., Dong, G.H., 2015. Experimental study on flow velocity and mooring loads for multiple net cages in steady current. Aquac. Eng. 67, 24–31. Elsevier. https://doi.org/10.1016/j.aquaeng.2015.05.005.

Zhu, L., Li, Z., Ketola, T., 2011. Biomass accumulations and nutrient uptake of plants cultivated on artificial floating beds in chinas rural area. Ecol. Eng. 37 (10), 1460–1466. Elsevier B.V. https://doi.org/10.1016/j.ecoleng.2011.03.010.

Zhu, L., Huguenard, K., Zou, Q., Fredriksson, D.W., Xie, D., 2020. Aquaculture farms as nature-based coastal protection : Random wave attenuation by suspended and submerged canopies. Coast. Eng. 160 (October 2019), 103737. Elsevier B.V. https://doi.org/10.1016/j.coastaleng.2020.103737.

Zhu, L., Lei, J., Huguenard, K., Fredriksson, D.W., 2021. Wave attenuation by suspended canopies with cultivated kelp (Saccharina latissima). Coast. Eng. 168 (June), 103947. Elsevier B.V. https://doi.org/10.1016/j.coastaleng.2021.103947.